Res Chem Intermed
https://doi.org/10.1007/s11164-018-3360-x

Catalytic behavior of magnetic Ni–Zn alloy

K. Dhanapal[1] · **S. Dhanavel**[1] · **T. A. Revathy**[1] · **V. Narayanan**[2] ·
A. Stephen[1]

Received: 5 October 2017 / Accepted: 1 March 2018

Abstract Ni–Zn alloy with various compositions of zinc was synthesised using a sodium borohydride-assisted chemical reduction method. The as-synthesised Ni–Zn alloy samples were annealed at 673 K for 2 h in nitrogen atmosphere. The atomic absorption spectroscopy measurement reveals the zinc-rich composition in all alloy samples. Field emission scanning electron microscopy shows that the surface morphology of Ni–Zn alloys has a flake-like nature. The X-ray diffraction pattern of as-synthesised samples shows the presence of nickel hydroxide while the annealed samples show formation of Ni_2Zn_{11} phase. The phase transition temperature of as-synthesised Ni–Zn alloy was observed using differential scanning calorimetry and crystallization temperature changes with zinc composition was also examined. The room temperature magnetic behaviour of both as-synthesised and annealed samples was studied using vibrating sample magnetometer. This shows that as-synthesised samples have a weak ferromagnetic nature and annealed samples have a soft ferromagnetic nature. The decreasing magnetization value and Curie temperature with zinc composition was observed. The catalytic activity of Ni–Zn alloy was studied for the reduction of 4-nitrophenol. The rate constant value changes with zinc composition in the alloy.

Keywords Chemical reduction · Phase transition · Magnetic study · Catalytic activity

---

✉ A. Stephen
stephen_arum@hotmail.com

[1] Department of Nuclear Physics, University of Madras, Guindy Campus, Chennai 600 025, India

[2] Department of Inorganic Chemistry, University of Madras, Guindy Campus, Chennai 600 025, India

Introduction

Nanostructured magnetic alloys have attracted large interest in recent years due to their improved physical, magnetic and catalytic properties. These properties, exhibited by nano-sized materials, are excellent when compared to their bulk form. These properties lead to applications such as magnetic fluids, magnetic sensors, high density magnetic storage and environmental remediation [1–4]. Nickel-based binary and ternary alloys receive much interest due to their catalytic and corrosion resistance properties. The combination of nickel with non-magnetic metals is of great interest due to their enhanced properties, for example Ni–Zn [5], Ni–Sn [6], Ni–Cu [7] and Ni–Ag [8] systems are such types of alloys with added applications.

There are different methods available for the synthesis of these types of alloy, among which some important methods are hydro/solvo-thermal, electrodeposition, polyol process, mechanical alloying, micro-emulsion system, spray pyrolysis and chemical reduction [2, 8–10]. Normally, the chemical reduction method doesn't involve costly reagents and costly instruments to synthesis these alloys. The sodium borohydride-assisted chemical reduction method is employed for the preparation of Ni–Zn alloy. This method is preferred as it can produce nanosized alloys with the desired composition and in large quantity. The major advantage of sodium borohydride is that it can produce 8 mol of electrons from 1 mol, and it can reduce the metal ions in different types of medium [11–13].

4-Nitrophenol (4NP) is the most common pollutant present in industrial and agricultural waste water [14, 15]. This pollutant has to be removed or converted into some other form, as it is a toxic material. There are many methods available to remove this pollutant such as photo-catalytic degradation, electro-fenton method, microbial degradation, adsorption, microwave-assisted catalytic oxidation, electro-chemical treatment, metal catalysis [14]. The effective method is converting 4NP into 4-aminophonal (4AP) using a metal catalyst. This conversion takes place by the presence of a metal catalyst with sodium borohydride as the reducing agent. The by-product 4AP is an important intermediate material required for the preparation of analgesic and antipyretic drugs. 4AP is also used as photographic developer, hair dyeing agent, corrosion inhibitor in paints, anti-corrosion lubricating agent in fuel for two-cycle engines [16–18]. There are several noble metal catalysts available such as Pd, Au, Ag and Pt-Ni, but these catalysts are very expensive. The conventional method for hydrogenation of 4NP involves iron/acid as a reducing agent, but these produce huge amounts of sludge. The sodium borohydride-assisted chemical reduction method leads to the development of an environmentally friendly and cost effective catalyst [16, 19]. In addition to this, Ni-based alloys have the added advantage that they are magnetically recoverable, which increases the recyclability of the alloy as a catalyst for the reduction of 4NP to 4AP.

Experiment

The Ni–Zn alloys were synthesised using a conventional sodium borohydride-assisted chemical reduction method. The polyvinylpyrrolidone (PVP) was purchased from Sigma Aldrich, and all other chemicals were from Merck India. The Ni–Zn alloy was prepared with different concentrations of zinc and nickel in the electrolyte. The molarity of zinc was varied at 0.02, 0.05, 0.1 and 0.15 M with respect to the nickel, resulting in a total molarity of 0.2 M in 50 mL of distilled water. The aqueous solution was prepared using nickel chloride and zinc chloride. The solution was stirred for 20 min after the addition of capping agent PVP of 0.05 M in 50 mL. The 0.1 M of sodium borohydride was added to the aqueous solution drop wise via burette. The aqueous solution colour changes from light green to black by the addition of sodium borohydride, confirming the reduction of metal ions. Then the precipitate was washed 6 times with distilled water and finally with acetone. The chemical reaction involved while reducing metal ions through sodium borohydride is given below.

$$\mathrm{NiSO_4 + 2NaBH_4 \rightarrow Ni + H_2 + B_2H_6 + Na_2SO_4}$$
$$\mathrm{ZnCl_2 + 2NaBH_4 \rightarrow Zn + H_2 + B_2H_6 + 2NaCl}$$

The Ni–Zn alloy was synthesised with four different electrolyte concentration ratios: (i) Ni 90:Zn 10 (Sample A), (ii) Ni 75:Zn 25 (Sample B), (iii) Ni 50:Zn 50 (Sample C) and (iv) Ni 25:Zn 75 (Sample D). Pure nickel was also synthesised using similar methodology.

The as-synthesised Ni–Zn alloy was annealed in nitrogen atmosphere for 2 h at 673 K. The as-synthesised and annealed samples were subjected to the following characterizations. The composition of individual elements present in the alloy was measured from atomic absorption spectroscopy (AAS, Perkin Elmer AAS 700). The morphology of the annealed samples was observed using field emission scanning electron microscopy (FE-SEM, FEI Quanta FEG 200). The crystalline nature of both as-synthesised and annealed samples was measured using powder X-ray diffraction (XRD, 3003 TT). Differential scanning calorimetry (DSC, Perkin Elmer Optima 5300 DV) was used to observe the phase transition in the alloy while heating. Vibrating sample magnetometry (VSM, Lakeshore VSM 7410) was employed to know the magnetic behaviour of both as-synthesised and annealed Ni–Zn alloy. The catalytic behaviour of alloy was observed using UV–Vis spectrometer (Analytik Gena, Specord 210plus).

Results and discussion

Composition analysis

The composition of nickel and zinc in the alloy was measured using AAS. The percentage of nickel and zinc present in the alloy are given in Table 1. The measured composition is more than the initial electrolyte composition. In sample A,

Table 1 Composition of Ni–Zn alloy

S. no	Sample code	Nickel (%)	Zinc (%)
1	Sample A	76.89	23.11
2	Sample B	66.88	33.12
3	Sample C	42.79	57.21
4	Sample D	19.59	80.41

the observed composition of zinc is twice as the electrolyte composition. Even though the standard reduction potential of zinc is high when compared to nickel, the percentage of zinc is high in the Ni–Zn alloy. A maximum difference of 13.11 wt% of zinc is observed in sample A while a minimum of 5.41 wt% difference is observed in sample D. The reason for this excess percentage of zinc in the alloy, is the anomalous reduction mechanism. At first Ni^{2+} is reduced which chemisorbs water molecule to form $Ni(OH)^{+}$, suppressing the further reduction of Ni^{2+} leading to the preferential reduction of Zn^{2+} in the overall reduction process [20, 21]. This reveals the minimum difference between the initial and final composition in sample D.

Surface morphology

The surface morphology of annealed Ni–Zn alloy was observed using FESEM. The morphology of pure nickel, samples A, B, C and D are represented in Fig. 1. Pure nickel shows agglomerated particles with a foam-like nature whereas sample A shows a sheet-like nature. In the case of sample B, a densely packed foam-like nature can be viewed. A further increase of the percentage of zinc in nickel changes this foam-like nature to the flakes of sample C. As the percentage of zinc increases,

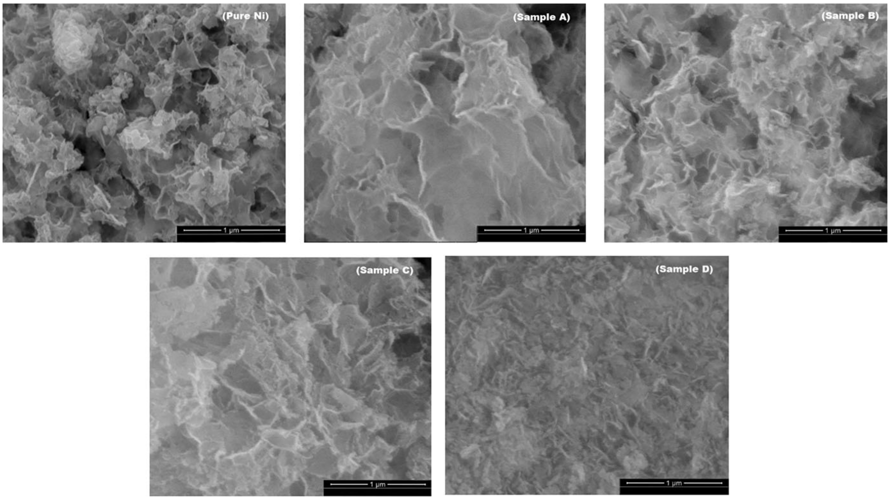

Fig. 1 Surface morphology of Ni–Zn alloy

the foam-like nature changes to a densely packed nature. This further decreases the flake size and appears like tightly packed flake particles in sample D.

Structural information

The structural information of the Ni–Zn alloy was deduced from the XRD pattern. The XRD pattern of both as-synthesised and annealed samples are shown in Figs. 2 and 3. The XRD pattern of as-synthesised nickel shows an amorphous nature with a broad peak around 44°. The XRD pattern of samples A, B, C and D shows two main diffraction peaks at 34° and 60°. These diffraction peaks correspond to $Ni(OH)_2$ with reference to the JCPDS file number 01-1047.

XRD patterns of the annealed samples show a different set of diffraction peaks when compared to the as-synthesised samples. Pure nickel shows the diffraction peaks at 44°, 52° and 76°, indexed to planes (111), (200) and (220), respectively, corresponding to nickel in the *fcc* phase with space group Fm-3 m, with reference to JCPDS file number 65-2865. Sample B shows diffraction peaks corresponding to both pure nickel and the Ni_2Zn_{11} phase with reference to JCPDS file number 65-5310. Both Ni_2Zn_{11} and $Zn(OH)_2$ phase is observed in the sample C. The $Zn(OH)_2$ phase is confirmed with JCPDS file number 48-1066. The XRD pattern confirms that the Ni_2Zn_{11} alloy phase observed in samples B and C. The presence of $Zn(OH)_2$ alone is observed in the case of sample D.

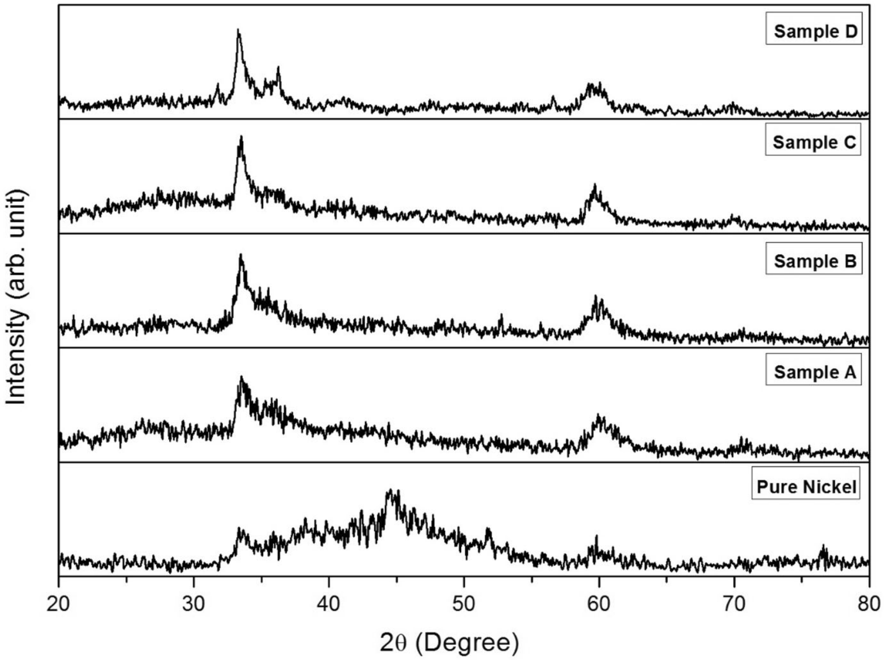

Fig. 2 XRD pattern of as-synthesised Ni–Zn alloy

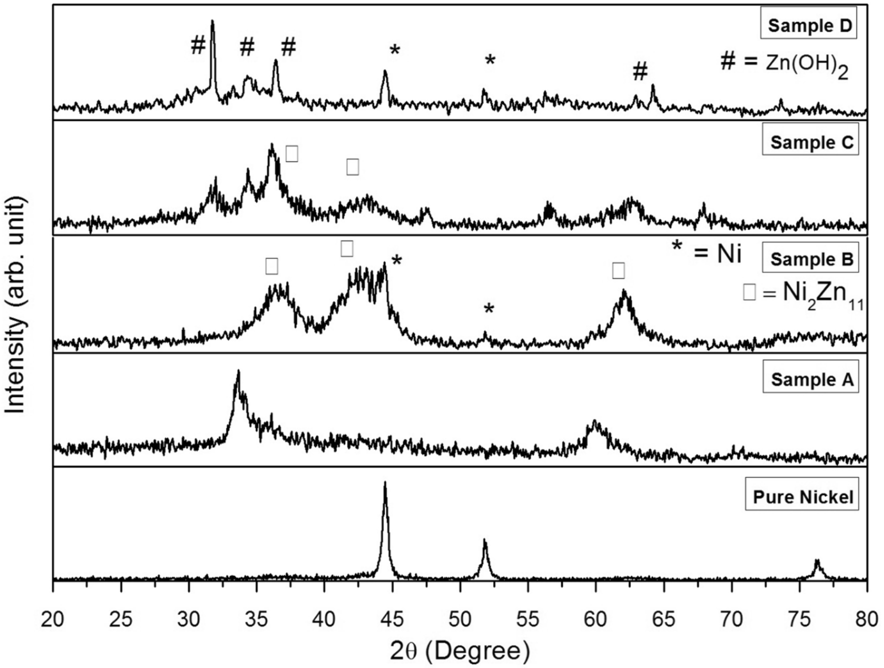

Fig. 3 XRD pattern of annealed Ni–Zn alloy

Phase transition

The phase transitions in the Ni–Zn alloy during heat treatment were analyzed in DSC. The DSC curve of samples B and C is shown in Fig. 4. The curve exhibits the presence of both endothermic and exothermic peaks, which confirm the structural

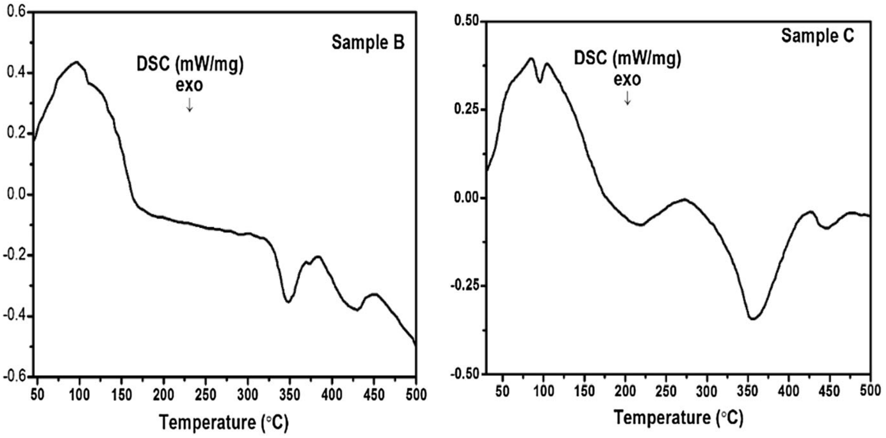

Fig. 4 DSC curve of Ni–Zn alloy

changes while heating. The endothermic peak is observed due to hydrogen desorption. It is well known that the inclusion of hydrogen is unavoidable co-process of chemical reduction [22, 23]. The exothermic peaks are de-convoluted and represented in Fig. 5. The de-convoluted peak maxima and their corresponding enthalpy values are given in Table 2. In the case of sample B, four exothermic peaks are observed: the first two peaks correspond to the precipitation of nickel [24]. The third peak at 413 °C is attributed to the structural relaxation, and the fourth peak at 430.9 °C corresponds to the phase formation of Ni_2Zn_{11} alloy [25, 26].

The sample C shows the similar phase transition with variation in the temperature range of 10 °C. The peak at 213.9 °C in sample C is due to removal of hydroxide which leads to the structural relaxation in the alloy. The enthalpy of Ni–Zn alloy phase formation varies from 2.4 J/g to 5.3 J/g with respect to the zinc composition.

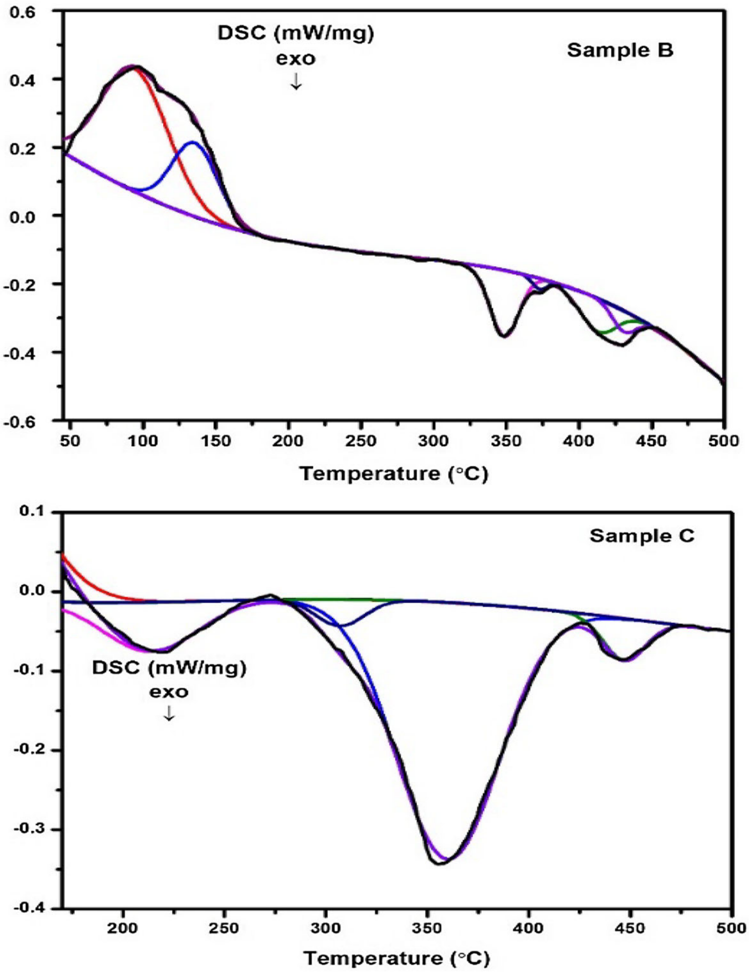

Fig. 5 De-convoluted DSC curve Ni–Zn alloy

Table 2 Exothermic peak position and enthalpy values of Ni–Zn alloy

Sample	Peak position (°C)	Enthalpy (J/g)
Sample B	348.5	12.5
	372.9	1.0
	413.1	8.0
	430.5	3.2
Sample C	213.8	5.6
	307.0	1.6
	360.0	33.1
	446.9	2.2

Magnetic behaviour

The magnetic behaviour of Ni–Zn alloys were studied using VSM. The room temperature hysteresis loop was taken for both as-synthesised and annealed samples. The hysteresis loops of both as-synthesised and annealed samples are shown in Figs. 6 and 7. The shape of hysteresis loop of as-synthesised samples represents a weak ferromagnetic nature in all the samples. The hysteresis loop of the annealed samples shows soft ferromagnetic nature in samples A, B and C, whereas sample D shows a weak ferromagnetic nature.

The saturation magnetization, coercivity, retentivity, M_r/M_s and hysteresis loss values are tabulated in Table 3. The saturation magnetization value of sample A is 3.10 emu/g, which is less than pure nickel. Samples B and C show saturation magnetization value 2.27 and 2.05, respectively. There is a large moment variation from sample C to D of nearly 11%. The reduction in saturation magnetization would be the addition of zinc in the alloy. In sample A, the addition of zinc in nickel

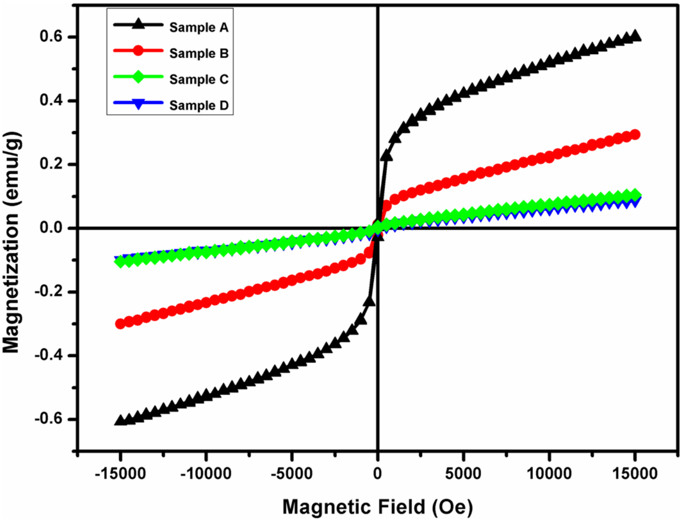

Fig. 6 Hysteresis loop of as-synthesised Ni–Zn alloy

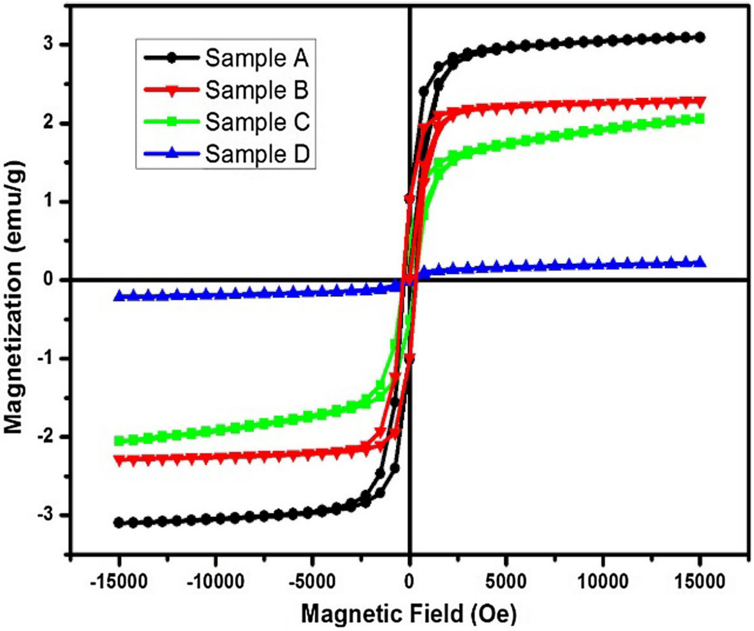

Fig. 7 Hysteresis loop of annealed Ni–Zn alloy

Table 3 Magnetic parameter values of annealed Ni–Zn alloy

Parameter	Sample A	Sample B	Sample C
M_s (emu/g)	3.10	2.27	2.05
H_c (Oe)	300	340	295
M_r (emu/g)	1.02	1.02	0.53
M_r/M_s (no unit)	0.33	0.45	0.26
Loss (erg/g cycle)	3486	3010	2215

matrix reduces the Ni–Ni interaction with a domination of Ni–Zn interaction results the lower saturation magnetization value. As the zinc composition increases the saturation magnetization values reduces for sample B and sample C. In the case of sample D, a weak ferromagnetism is observed due to the presence of a large amount Zn as evidenced from compositional analysis.

The retentivity value also reduces with the zinc composition from 1.02 emu/g for sample A to 0.53 emu/g for sample C. This shows that the increasing composition of zinc reduces the magnetic behaviour of the nickel without changing the ferromagnetic behaviour up to certain critical composition after which it becomes weakly ferromagnetic. The M_r/M_s ratio shows that the domains present in the samples are of pseudo single domain type [27, 28]. The hysteresis loss decreases with increasing zinc composition in the alloy.

The thermo-magnetic behaviour of the Ni–Zn alloy was studied using high temperature VSM measurement. The temperature versus magnetization graph (*M*–

T) of samples A and C are shown in Fig. 8. The *M*–*T* curve was measured in constant with magnetic field of 250 Oe. The *M*–*T* curve shows a gradual fall in the magnetic moment of the samples and shows absence of sharp transition in the magnetic moment. The moment of both the samples tend to zero after 350 °C and beyond that there is no variation in the magnetic moment. This confirms the paramagnetic nature of sample A and sample C after Curie transition. The first derivative of *M*–*T* curve is calculated and presented in the inset of Fig. 8 to determine the Curie temperature.

The Curie transition temperature is calculated from *M*–*T* curve and found to be 346 and 310 °C for sample A and sample C, respectively. The curie temperature of sample A is less than that of pure Ni, which is due to the incorporation of Zn atoms in the alloy there by decreasing the Curie temperature. Similarly, for sample C, further reduction in the Curie temperature is found, where the amount of Zn present in the alloy is higher than sample A. This confirms that there is a decrease in the Curie transition temperature of Ni–Zn alloy with increasing Zn composition in the alloy.

Catalytic activity

The catalytic behaviour of all the annealed samples was evaluated by the reduction of 4NP to 4AP in the presence of $NaBH_4$. The advantage of catalytic reduction of 4NP is that it can easily be monitored using the UV–Vis spectrophotometer. The absorption peak observed at 317 nm is due to 4NP, which is shifted to 400 nm after the addition of $NaBH_4$. In this process, the addition of $NaBH_4$ forms 4-nitrophenolate ions in the alkaline condition transforming light yellow colour of 4NP to the dark yellow colour. The absorption peak intensity at 400 nm shows no variation for several days, which shows the addition of $NaBH_4$ alone doesn't reduce the 4NP [14, 19]. The addition of an alloy catalyst in this solution shows a drastic decrease in the absorption peak within a short time period.

The catalytic reduction of all the samples is shown in the Fig. 9. In all the samples the reduction of 4NP to 4AP is observed. The absorption peak intensity at

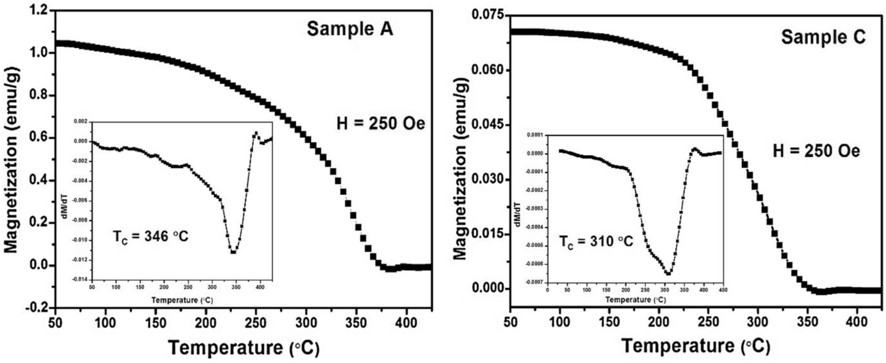

Fig. 8 *M*–*T* curve of Ni–Zn alloy

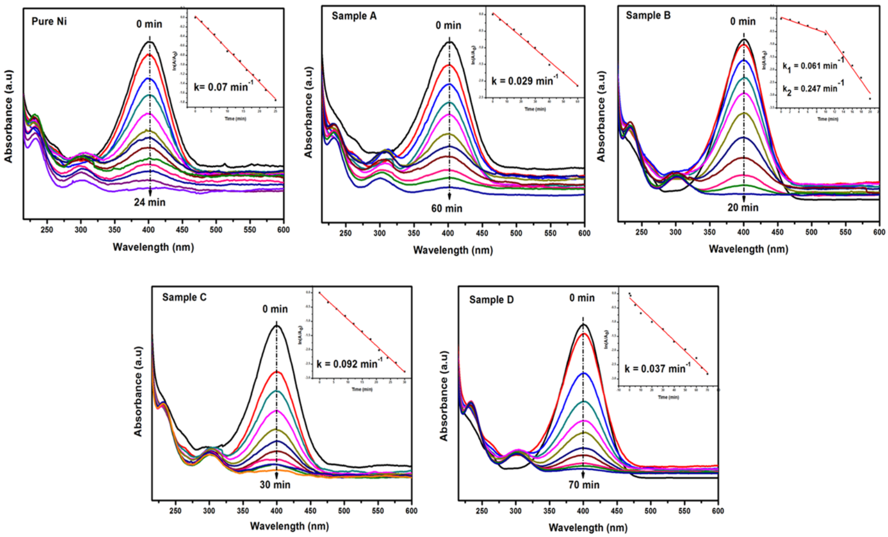

Fig. 9 Catalytic activity of Ni–Zn alloy

400 nm decreases with time, thereby increasing the intensity of the absorption peak at 300 nm, which is due to the 4AP. The spectrum shows that the reduction process starts immediately after the addition of a metal catalyst. This shows the absence of oxide in the material, otherwise there would have been some induction time. To avoid this, mostly nitrogen purging is used, but this is not used in this study as our alloy doesn't contain any oxide, while 4NP bubbles are decreased, which ensures that the metal catalysts are distributed uniformly during the reduction process [16, 29].

In order to investigate the reaction kinetics and rate constant, a time-dependent absorption graph was plotted for all samples and is shown in the inset of Fig. 9. The figures show that there is a faster reduction in the sample B when compared to all other samples. The curve represents the reduction process follows pseudo first order kinetics. The rate constant is calculated from the graph as, 0.07, 0.029, 0.092 and 0.037 min^{-1} for pure Ni, sample A, sample C and sample D, respectively. In sample B reduction was observed with two rate constants, which are 0.061 and 0.247 min^{-1}. This shows that sample B has higher catalytic activity when compared to other samples; this may be due to the densely packed foam-like nature of the sample B as evident from FESEM measurement.

The catalytic activity of all the samples was carried out at different pH values (4.0, 7.0 and 9.0). There is no significant variation in the activity. Hence, pH 7.0 is chosen for all studies. The reusability of the catalyst was carried out for five cycles, which is shown in Fig. 10. The catalyst retains its catalytic performance up to two cycles and further shows slight variation in the activity. The schematic representation of magnetic recoverability of the catalysts is also shown in Fig. 10.

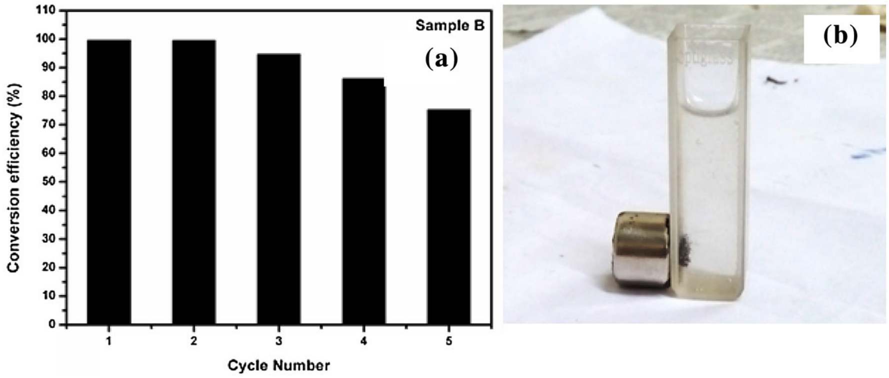

Fig. 10 Reusability of the catalyst

Conclusion

The Ni–Zn alloy was successfully synthesised using sodium borohydride-assisted chemical reduction. AAS analysis confirms the zinc-rich composition in all alloy samples. The surface morphology of alloy was transformed from foam-like to closely packed flakes as the zinc composition increased. The Ni_2Zn_{11} phase is observed in annealed Ni–Zn alloy from XRD measurement. The phase transition in the as-synthesised Ni–Zn alloy was analysed using DSC. The room temperature magnetic behaviour was observed from VSM. The hysteresis loop confirms the weak ferromagnetic nature in as-synthesised samples and soft ferromagnetic nature in annealed samples with dependence of saturation magnetization value in zinc composition. The catalytic activity of Ni–Zn alloy was studied towards the reduction of 4NP to 4AP. All samples show catalytic activity, and sample B shows better catalytic activity than other samples. Sample B has rate constants of 0.061 and 0.247 min^{-1}.

Acknowledgements Author (KD) would like to acknowledge NCNSNT, University of Madras for financial support. Authors also acknowledge IITM for FESEM, DSC and VSM measurement.

References

1. A.C. Hegde, K. Venkatakrishna, N. Eliaz, Surf. Coat. Technol. **205**, 2031 (2010)
2. Y. Pei, G. Zhou, N. Luan, B. Zong, M. Qiao, F. Tao, Chem. Soc. Rev. **41**, 8140 (2012)
3. Y. Chen, L. Wang, W. Wang, M. Cao, Appl. Catal. B **209**, 110 (2017)
4. Y. Chen, L. Wang, W. Wang, M. Cao, Mater. Chem. Phys. **199**, 416 (2017)
5. A.M. Alfantazi, J. Page, U. Erb, J. Appl. Electrochem. **26**, 1225 (1996)
6. Y.D. Yao, Y.Y. Chen, S.J. Tzeng, T.H. Chuang, Physica Status Solidi (a) **121**, 213 (1990)
7. I. Alstrup, J. Catal. **109**, 241 (1988)
8. K. Santhi, E. Thirumal, S.N. Karthick, H.-J. Kim, M. Nidhin, V. Narayanan, A. Stephen, J. Nanopart. Res. **14**, 1 (2012)
9. M.A. Willard, L.K. Kurihara, E.E. Carpenter, S. Calvin, V.G. Harris, Int. Mater. Rev. **49**, 125 (2004)
10. M.R. Knecht, M.G. Weir, A.I. Frenkel, R.M. Crooks, Chem. Mater. **20**, 1019 (2008)
11. J. Lu, D.B. Dreisinger, W.C. Cooper, Hydrometallurgy **45**, 305 (1997)

12. Y. Yamauchi, T. Yokoshima, T. Momma, T. Osaka, K. Kuroda, J. Mater. Chem. **14**, 2935 (2004)
13. Z. Hu, Y. Hsia, J. Zheng, J. Shen, Q. Yan, L. Dai, J. Appl. Phys. **70**, 436 (1991)
14. Y.-C. Chang, D.-H. Chen, J. Hazard. Mater. **165**, 664 (2009)
15. J. Feng, L. Su, Y. Ma, C. Ren, Q. Guo, X. Chen, Chem. Eng. J. **221**, 16 (2013)
16. S. Saha, A. Pal, S. Kundu, S. Basu, T. Pal, Langmuir **26**, 2885 (2010)
17. K.-L. Wu, X.-W. Wei, X.-M. Zhou, D.-H. Wu, X.-W. Liu, Y. Ye, Q. Wang, J. Phys. Chem. C **115**, 16268 (2011)
18. S. Dhanavel, N. Manivannan, N. Mathivanan, V.K. Gupta, V. Narayanan, A. Stephen, J. Mol. Liq. **257**, 32 (2018)
19. Z. Jiang, J. Xie, D. Jiang, J. Jing, H. Qin, CrystEngComm **14**, 4601 (2012)
20. M.M. Abou-Krisha, F.H. Assaf, S.A. El-Naby, J. Coat. Technol. Res. **6**, 391 (2009)
21. A. Petrauskas, L. Grincevičienė, A. Češūnienė, R. Juškėnas, Electrochim. Acta **50**, 1189 (2005)
22. A. Stephen, F. Rossi, L. Nasi, C. Ferrari, N. Ponpandian, M.V. Ananth, V. Ravichandran, J. Appl. Phys. **103**, 053511 (2008)
23. S. Harada, T. Sohmura, F.E. Fujita, J. Phys. F Met. Phys. **13**, 1429 (1983)
24. K. Dhanapal, V. Narayanan, A. Stephen, Mater. Chem. Phys. **166**, 153 (2015)
25. X. Su, N.-Y. Tang, J. Toguri, JPE **23**, 140 (2002)
26. G. Vassilev, T. Gomez-Acebo, J.-C. Tedenac, JPE **21**, 287 (2000)
27. A.P. Roberts, C.R. Pike, K.L. Verosub, J. Geophys. Res. Solid Earth **105**, 28461 (2000)
28. A.R. John, P. Arumugam, Chem. Eng. J. **243**, 436 (2014)
29. S. Wunder, F. Polzer, Y. Lu, Y. Mei, M. Ballauff, J. Phys. Chem. C **114**, 8814 (2010)